

Photovoltaic properties of metal-narrow-gap semiconductor contacts**

The mechanisms of photovoltage spectra creation (photon flux distributions and photoexcitation processes) in metal-semiconductor contact are discussed. A special interest is devoted to metallic contact on narrow-gap semiconductor. The application of photovoltage measurements to investigations of metal-(p)Cd_xHg_{1-x}Te contact properties is also described.

1. Introduction

Measurements of photocurrent or photovoltage spectrum in rectifying metal-semiconductor contacts have been commonly used for the determination of contact potential barrier. This spectrum is, in general, due to excitation of current carriers from metal to the conduction or valence band. However, this method is hardly applied to contacts with narrow-gap semiconductor in which the commonly appearing inequality $E_g > \Phi_B$ (energy gap E_g greater than barrier height Φ_B) is not satisfied. In this contact the usually stated relation $E_g < \Phi_B$ leads to rising of the inverted layer near semiconductor surface. The electrical properties of these contact (to semiconductor with inverted surface) are clearly different from the common Schottky devices (see e.g. [1, 2]).

In this work we discussed the mechanisms of photovoltage (PV) spectra formation in contacts to both wide- and narrow-gap semiconductors, and with the application of PV-measurements to investigations of metal-(p)Cd_xHg_{1-x}Te (narrow-gap semiconductor) contact properties.

2. Simple theory of PV-creation

In this part the photovoltage formation will be discussed in metal contact to *p*-type semiconductors with holes as the majority carriers. It is well known that for the contact to *n*-type material the situation is analogical, i.e. band diagram is exactly inverted and all the mechanisms discussed are attributed to the electrons. The *p*-type semiconductors has been selected for examination having in mind the application of metal contact to *p*-type Cd_xHg_{1-x}Te.

* Institute of Physics, Wrocław Technical University, Wrocław, Poland.

** Work sponsored by Wrocław Technical University under contract 60/75 (IM-116).

2.1. Photon flux distributions

2.1.1. Wide-gap semiconductor

Schematic energy band diagram (SEBD) of contact to *p*-type wide-gap semiconductor is shown in fig. 1. It is easily observed that three fundamental processes can occur:

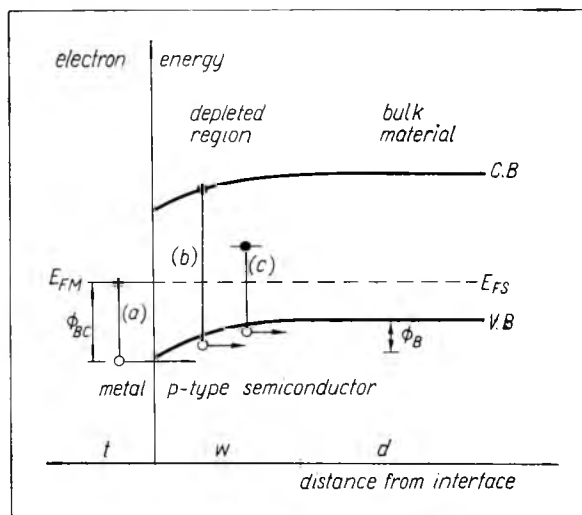


Fig. 1. Schematic energy band diagram of metallic contact to wide-gap *p*-type semiconductor (explanation — see text)

a) Emission of photoexcited holes from the Fermi level of metal to the valence band of the *p*-type semiconductor for $h\nu \cong \Phi_{BC}$.

b) Band-to-band excitation of hole-electron pairs in depleted or bulk-material regions in semiconductor for $h\nu \cong E_g$.

c) Excitation from deep acceptor centers to the valence band, for $h\nu$ equal to acceptor level energy (when the participation of interface states can be neglected).

In fig. 1 Φ_{BC} denotes the total barrier height calculated (for holes from the metal) from a well-known simple Schottky equation

$$\Phi_{BC} = \chi - \varphi_m + (E_g + E_F) - \Delta\Phi \quad (1)$$

where χ is an electron affinity of semiconductor, φ_m is a work-function of metal, E_g is an energy gap, E_F is a Fermi level (from top of the valence band), and $\Delta\Phi$ is a barrier lowering due to image-mirror forces (Schottky effects). The Φ_B value denotes the barrier height for holes from semiconductor, and $\Phi_{BC} = \Phi_B + E_F$, w and d denote the width of depleted and bulk-material regions, respectively.

The description of radiation interaction with metal-semiconductor contact requires the knowledge of the distribution of photon flux in different regions. Schematic pictures of the structure investigated when monochromatic radiation is incident upon the metal and passes through the interface to the semiconductor, and vice versa, are presented in fig. 2a and b, respectively. In fig. 2a and b t denotes the metal-semitransparent layer thickness.

If the photon flux incident upon the metal (fig. 2a) is $I_0/h\nu$ and leaves the metal as $I/h\nu$ (for the contact investigated the exact relation between I_0 and I is

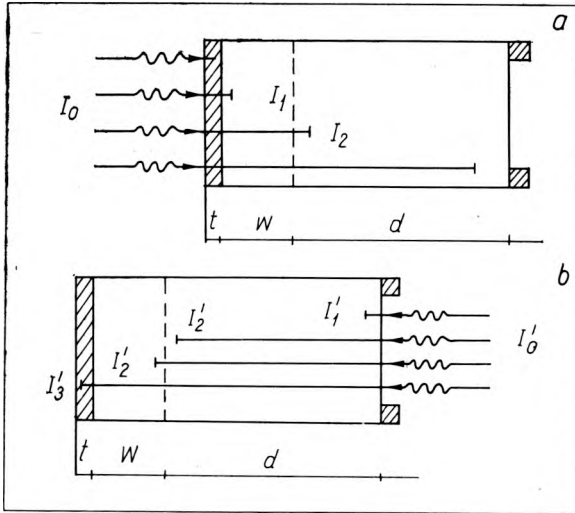


Fig. 2. Schematic photon flux distribution in both a front-wall (a), and back-wall (b) geometry of contract illumination

at present unknown being mainly the function of reflection coefficient and thickness of metal semitransparent layer), then photon flux which entered the region w is given by

$$\frac{I_1}{h\nu} = (1-R) \frac{I}{h\nu}, \quad (2)$$

where R is a reflection coefficient of semiconductor (inner reflections in metal are neglected).

The photon flux enters the region d

$$\begin{aligned} \frac{I_2}{h\nu} &= \frac{I_1}{h\nu} \exp(-\alpha_d w) \\ &= (1-R) \frac{I}{h\nu} \exp(-\alpha_d w), \end{aligned} \quad (3)$$

where α_d is the absorption coefficient in depleted region.

If the photon flux incident upon the semiconductor (fig. 2b) is $I'_0/h\nu$, then the photon flux which entered the region d is given by the formulae

$$\frac{I'_1}{h\nu} = (1-R) \frac{I'_0}{h\nu}, \quad (4)$$

and into region w by

$$\frac{I'_2}{h\nu} = \frac{I'_1}{h\nu} \exp(-\alpha d) = (1-R) \frac{I'_0}{h\nu} \exp(-\alpha d), \quad (5)$$

where α is the absorption coefficient in bulk material, and into metal by

$$\begin{aligned} \frac{I'_3}{h\nu} &= \frac{I'_2}{h\nu} \exp(-\alpha_d w) \\ &= (1-R) \frac{I'_0}{h\nu} \exp(-\alpha_d w - \alpha d). \end{aligned} \quad (6)$$

If absorption coefficients in both depleted and bulk-material regions are equal ($\alpha_d = \alpha$), then

$$\frac{I'_3}{h\nu} = (1-R) \frac{I'_0}{h\nu} \exp[-\alpha(d+w)]. \quad (7)$$

The inner reflections between the regions w and d may be neglected.

2.1.2. Narrow-gap semiconductor

SEBD of contact to p -type narrow-gap semiconductor including the inverted, depleted and bulk-material regions is shown in fig. 3. Besides the photoexcitation processes (shown in fig. 1) an additional process, i.e. excitation of hole-electron pairs can occur

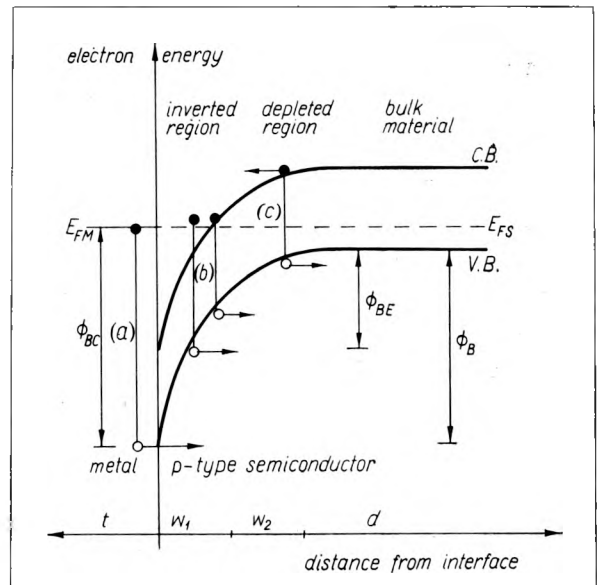


Fig. 3. Schematic energy band diagram of metallic contact to narrow-gap p -type semiconductor (explanation — see text)

in inverted region of semiconductor for $E_g \leq h\nu \leq \Phi_B$, with absorption coefficient being relatively greater due to free-carriers absorption (comp. (b) – 2.1.1). In fig. 3, for simplicity the excitations from deep levels are eliminated. Φ_{BE} denotes the barrier height obtained experimentally*. In this case the photons flux distribution will be changed.

If the photons flux falling on the metal (see fig. 3 and 2a for comparison) enters the region w_1 , its behaviour is described by eq. (2) while that entering region w_2 is given by

$$\begin{aligned} \frac{I_2}{h\nu} &= \frac{I_1}{h\nu} \exp(-a_i w_1) \\ &= (1-R) \frac{I}{h\nu} \exp(-a_i w_1) \end{aligned} \quad (8)$$

where a_i is the absorption coefficient in inverted region. The photon flux entering the region d satisfies the following relation:

$$\begin{aligned} \frac{I_3}{h\nu} &= \frac{I_2}{h\nu} \exp(-a_d w_2) \\ &= (1-R) \frac{I}{h\nu} \exp(-a_i w_1 - a_d w_2). \end{aligned} \quad (9)$$

For energy higher than absorption edge in semiconductor the absorption coefficients in both regions are approximately equal ($a_i = a_d$) while for energy lower than the absorption edge, $a_i > a_d$. For $h\nu \geq E_g$ we have $a_d \cong a_i \cong a$ and

$$\frac{I_3}{h\nu} = (1-R) \frac{I}{h\nu} \exp(-aw). \quad (10)$$

The inner reflection between w_1 , w_2 and d regions may be neglected. It is easy to shown that if the photon flux falls upon the semiconductor surface the parts of it entering regions d and w_2 are described by formulae (4) and (5), respectively, while those entering the region w_1 and metal are given by the formulae

$$\begin{aligned} \frac{I'_3}{h\nu} &= \frac{I'_2}{h\nu} \exp(-a_d w_2) \\ &= (1-R) \frac{I'_0}{h\nu} \exp[-a(w_2 + d)], \end{aligned} \quad (11)$$

$$\begin{aligned} \frac{I'_4}{h\nu} &= \frac{I'_3}{h\nu} \exp(-a_i w_1) \\ &= (1-R) \frac{I'_0}{h\nu} \exp[-a(w + d)], \end{aligned} \quad (12)$$

respectively, if inner reflections in semiconductor are neglected and $a_i = a_d = a$.

* If the barrier height is obtained from current-voltage characteristics.

Now we must consider in detail the photoexcitation processes in different regions of contacts.

2.2. Photoexcitation processes

2.2.1. Photoexcitation in semiconductor

If the volume recombination velocities of electrons and holes are equal and dependent linear on their concentration, and when space charge in semiconductor may be neglected,

$$\Delta n = \Delta p = \Delta N = G\tau, \quad (13)$$

where Δn and Δp denote the concentrations of excess electrons and holes, respectively, G is a carrier-pairs-generation velocity and τ is a lifetime of excess carriers.

It may be shown (see e.g. [3]) that ΔN is equal to the photon absorption rate for given quantum photoexcitation efficiency* η if the surface recombination rate may be neglected and if the process of absorption occurs uniformly within the whole volume of the semiconductor. The last condition is described by

$$\Delta N = \tau\eta\alpha \frac{I_k}{h\nu} \exp(-ax), \quad (14)$$

where $I_k/h\nu$ is given by the respective equations (2)–(12).

On the other hand, for nonhomogeneous absorption on the x_0 way, ΔN is given by

$$\Delta N = \frac{1}{x_0} \int_0^{x_0} \Delta N(x) dx. \quad (15)$$

The photoexcitation processes which can occur in wide- and narrow-gap semiconductors are different. For the contact wide-gap material they are described in e.g. [4]. We shall consider below the narrow-gap case.

If the radiation falls on the semitransparent metal layer the number of carrier pairs generated according to the mechanism (b) (section 2.1.1) per unit time is given by

$$\Delta N_1 = \eta \int_0^{w_1} \alpha(1-R) \frac{I_0}{h\nu} \exp(-ax) dx, \quad (16a)$$

for the region w_1 and by

$$\begin{aligned} \Delta N_2 &= \eta \int_{w_1}^w \alpha(1-R) \frac{I_0}{h\nu} \times \\ &\times \exp(-aw_1) \exp(-ax) dx, \end{aligned} \quad (16b)$$

* Quantum efficiency is defined in practice as a ratio of generated carriers to incident photons. This value may be different in w_1 , w_2 (or w) and d regions, but in one region is approximately constant.

for region w_2 where the excitation mechanism (c) (section 2.1.1) takes place and finally by

$$\Delta N_3 = \eta \int_a^{w+d} \alpha(1-R) \frac{I_0}{h\nu} \times \exp(-aw) \exp(-ax) dx, \quad (16c)$$

for the region d at the presence of mechanism (c) (section 2.1.1) if

$$\alpha_i = \alpha_d = \alpha.$$

If the radiation falls on the semiconductor surface, the number of carrier pairs per unit time generated in d region due to (c) mechanism (section 2.1.1) is given by

$$\Delta N'_3 = \eta \int_0^d \alpha(1-R) \frac{I'_0}{h\nu} \exp(-ax) dx, \quad (17a)$$

in w_2 region by

$$\Delta N'_2 = \eta \int_a^{d+w_2} \alpha(1-R) \frac{I'_0}{h\nu} \times \exp(-ad) \exp(-ax) dx, \quad (17b)$$

and in w_1 region by

$$\Delta N'_1 = \int_{d+w_2}^{d+w} \alpha(1-R) \frac{I'_0}{h\nu} \times \exp[-a(w_2+d)] \exp(-ax) dx. \quad (17c)$$

From the comparison of eq. (16) with eq. (17) it follows that for the two methods of contact illumination both the photon flux distribution and intensities of photoexcitation processes will be different (see section 2.3).

2.2.2. Photoexcitation from metal over the barrier

This process, denoted by (a) in figs 1 and 3, is related to the height of the potential barrier Φ_{BC} , and was widely discussed, e.g. in [4], being based on Fowler carriers distribution [5].

If x -axis is normal to the metal-semiconductor interface, the holes number dH_x whose x -component of the momentum lies between p_x and $(p_x + dp_x)$, is given by

$$dH_x = \frac{2\pi k T m_h}{h^3} \ln \left[1 + \exp \left(- \frac{E_{kx}}{kT} \right) \right] dp_x, \quad (18)$$

where $E_{kx} = (p_x^2)/(2m_h) = 1/2(m_h V_x^2)$. It has been assumed, that such carriers are emitted from the Fermi level of metal to the semiconductor*, whose E_{kx}

* The probability of carriers tunneling is not considered by Fowler.

(augmented by $h\nu$) is greater than the potential barrier height Φ_{BC} , lowered by Schottky effect. The reference energy level is the Fermi level of the metal (or the semiconductor, in equilibrium). The x -axis component of current of those carriers is given by

$$dj_x = q(dH_x) V_x.$$

Orthewise (for $dp_x = m_h dV_x$)

$$j_x = \frac{4\pi k T q m_h^2}{h^3} \times \int_{V_{x0}}^{V_{x\infty}} V_x \ln \left[1 + \exp \left(- \frac{m_h V_x^2}{2kT} \right) \right] dV_x, \quad (19)$$

where V_{x0} is a minimum carrier velocity determined by

$$\frac{1}{2} m_h V_{x0}^2 + h\nu = \Phi_{BC}. \quad (20)$$

By calculating the integral in eq. (19) we obtain

$$j_x = \frac{4\pi q (kT)^2 m_h}{h^3} \times \left[\exp(\xi) - \frac{1}{2^2} \exp(2\xi) + \frac{1}{3^2} \exp(3\xi) - \frac{1}{4^2} \exp(4\xi) + \dots \right], \quad (21a)$$

for $h\nu \leq \Phi_{BC}$, and

$$j_x = \frac{4\pi q (kT)^2 m_h}{h^3} \times \left\{ A - \left[\exp(-\xi) - \frac{1}{2^2} \exp(-2\xi) + \frac{1}{3^2} \exp(-3\xi) - \frac{1}{4^2} \exp(-4\xi) + \dots \right] \right\} \quad (21b)$$

for $h\nu \geq \Phi_{BC}$, where $\xi = (h\nu - \Phi_{BC})/kT$. The term $A = \pi^2/6 + 1/2\xi^2$ binds together both series (21a) and (21b) at $h\nu = \Phi_{BC}$. Its value determines practically the j_x - current at $h\nu > \Phi_{BC} + nkT$, where $n \cong 5$, because of very small values the series in eq. (21b).

In detail:

$$\text{at } T = 0 \text{ K} \left\{ \begin{array}{l} j_x(0) = 0, \quad \text{for } h\nu < \Phi_{BC} \\ j_x(0) \cong \frac{4\pi q (kT)^2 m_h}{h^3} A = \frac{2\pi q m_h}{h^3} \times \\ \times (h\nu - \Phi_{BC})^2, \quad \text{for } h\nu \geq \Phi_{BC} \end{array} \right. \quad (22a)$$

and

$$\text{at } T > 0 \text{ K} \left\{ \begin{array}{l} j_x(T) \cong 0, \quad \text{for } h\nu < \Phi_{BC} - 5kT \\ j_x(T) = \frac{2\pi^3 q m_h}{3h^3} (kT)^2 + j_x(0) \\ = C(kT)^2 + \frac{2\pi q m_h}{h^3} (h\nu - \Phi_{BC})^2, \\ \text{for } h\nu \geq \Phi_{BC} + 5kT, \end{array} \right. \quad (22b)$$

at arbitrary temperatures.

The relations (21a) and (21b) are presented in figs 4a, b as a current-energy plot (fig. 4a), and a square root of current vs. photon energy (for $h\nu \geq \Phi_{BC}$) for several commonly used temperatures (fig. 4b). As shown in fig. 4, the commonly used relation

$$j_x(0) \sim (h\nu - \Phi_{BC})^2$$

is not justified for photons with $h\nu \cong \Phi_{BC}$ at $T > 0K$. It is easy to estimate the kT -values range, for which this

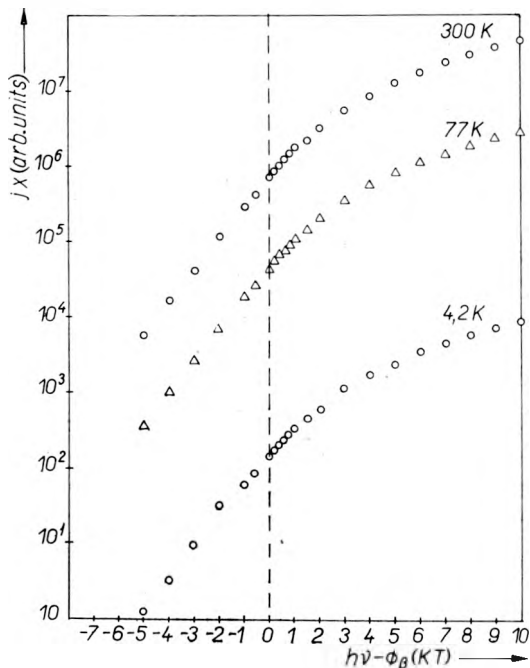


Fig.4a. Dependence of carriers current on photons energy

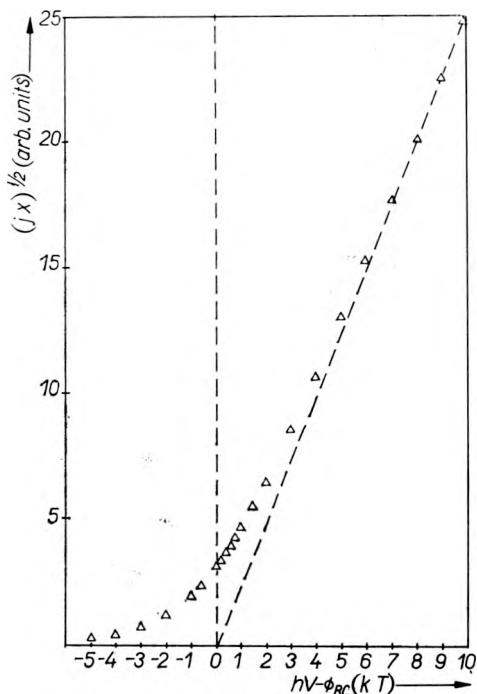


Fig. 4b. Dependence of square root of photoexcited current on photons energy for $h\nu \geq \Phi_{BC}$

relation is fulfilled. From fig. 4b it follows clearly that it is true for $h\nu \geq \Phi_{BC} + 5kT$ (term A prevails on the power series in eq. (21b)), and to obtain the true barrier height the thermal correction should be performed.

Because the total current density is proportional to the open-circuit photovoltage U_{Ph} (for low photovoltage), then

$$U_{Ph} \sim \eta \frac{I_0}{h\nu} (h\nu - \Phi_{BC})^2, \quad (23a)$$

or

$$\left(U_{Ph} \frac{h\nu}{I_0} \right)^{1/2} \sim (h\nu - \Phi_{BC}), \quad (23b)$$

always for $h\nu \geq \Phi_{BC} + 5kT$.

2.3. Limits of photovoltaic spectra

In the front-wall configuration (light falls upon the metal) the upper energy limit of photons (which enter next region) is determined by the barrier height value $h\nu \cong \Phi_{BC}$, and in the next regions, by the value of energy of electrons band-to-band generation. The lower energy limit is determined by band-gap value, $h\nu \cong E_g$, but the flux density of photons with this energy will be diminishing along their way (see eqs. (2), (8) and (9)). The wavelength range of photoresponse is relatively broad, in the first approximation it ranges from $\lambda_1(\mu m) = 1.24 \Phi_{BC}^{-1}$ (eV) to $\lambda_2(\mu m) = 1.24 E_g^{-1}$ (eV). In the opposite, in the back-wall geometry (radiation falls upon the semiconductor) both the upper and lower limits of photons energy (which will generate the photoresponse) are determined by band-gap value.

If consider, for example (for the metal-Cd_xHg_{1-x}Te contacts investigated — see section 3) the following values of parameters characterising the typical situation: $w_1 = w_2 = 50$ nm, $d = 100$ μm, $R = 0.3$, $(\alpha_i = \alpha_d = \alpha)_{min} = 2 \times 10^2$ cm⁻¹, $(\dots)_{max} = 2 \times 10^3$ cm⁻¹, and $\eta = 1$, then by solving the integrals from eqs. (16) and (17) we obtain schematic distribution of light-injected carriers for the contact investigated, presented in fig. 5 for both illumination geometries. It is clearly observed that due to overbarrier emission in barrier region, and to band-to-band excitations in w_1, w_2 and d regions the PV-response for the front-wall geometry will be generated in all the regions. In the latter region, however, the PV-response values are distinctly decreasing. The photoresponse spectrum in back-wall configuration will be simpler, the PV-response being produced by only one mechanism (in d region).

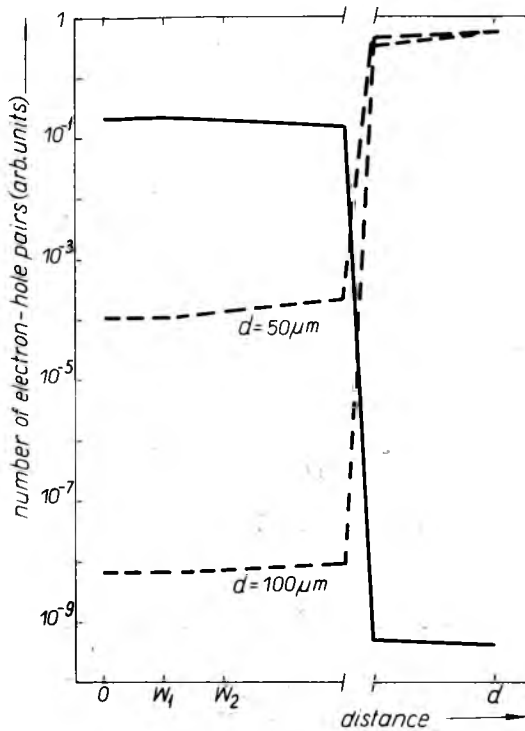


Fig. 5. Schematic distribution of light-injected carriers for metal-narrow gap semiconductor contact in cases of front-wall (full line), and back-wall (dashed line) geometries

On the other hand, in the case of very thin semiconductor (e.g. $d = 50 \mu\text{m}$) the PV -response can be produced in all the regions. It should be added, that if the contact region lies deep from semiconductor surface (d is greater than the diffusion length of carriers generated) then high absorption and generation of carriers take place near the semiconductor surface. Hence, only a small number of free carriers can diffuse into the contact region. Consequently, the PV -response drops markedly.

For these two methods of illumination the behaviour of contact to wide-gap material differs completely from that of contact to narrow-gap material, discussed above. Upper and lower limits are determined by the values of energy gap and barrier height, respectively, and the broad spectrum of photoresponse can be expected only for back-wall configuration.

3. Experiments on metal-(p) $\text{Cd}_x\text{Hg}_{1-x}\text{Te}$ contacts

In this section we describe deposition technology and geometry of the contact as well as the experimental setup for photovoltage measurement. Next the first experimental results of PV -measurements on $\text{Au}(p)\text{Cd}_x\text{Hg}_{1-x}\text{Te}$ contacts are shown.

The p -type $\text{Cd}_x\text{Hg}_{1-x}\text{Te}$ ($x \cong 0.2$) samples were cut by wire saw and etched in 5% solution of Br in methyl alcohol. The final plates were $70\text{--}300 \mu\text{m}$ thick. The metal (Au) contacts were evaporated in a vacuum of the order 10^{-5} Torr. The geometry of contact is presented in fig. 6a. The active area of contact measured was relatively large (up to 5 mm^2), while its thickness was small (about $3 \times 10^{-8} \text{ m}$) to make the metallic layer semi-transparent to the radiation. The electrodes were connected by indium soldering the Au -wire of 0.1 mm in diameter. For each semiconductor sample the Hall coefficient and conductivity were measured within the temperature range $77\text{--}300 \text{ K}$, the holes concentrations $(1\text{--}8) \times 10^{23} \text{ m}^{-3}$ have been obtained at 77 K .

The spectral measurements were performed at 300 K using the experimental arrangement composed of SiC -light source ($T \cong 1500 \text{ K}$) which was mechanically chopped at 10 Hz and monochromatized with a SPM-1 Zeiss monochromator. The setup used is shown in fig. 6b; it allows to obtain directly the ratio of photoresponses from the contacts investigated and reference detector. The PV -responses were measured by lock-in amplifier (Unipan 233), using the signal from a standard photodiode illuminated through the chopper as a command signal. In order to obtain the PV -response per unit photon flux, the incident light intensity $I_0(h\nu)$ was measured with a reference

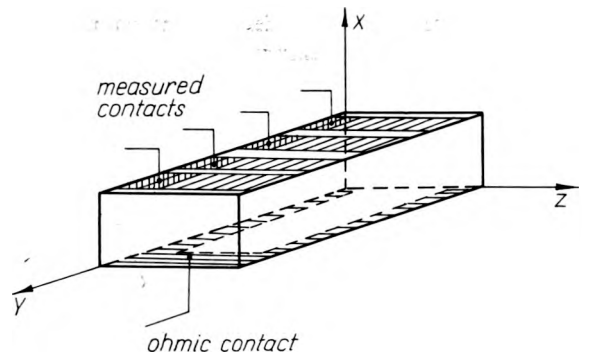


Fig. 6a. The geometry of $\text{Au-Cd}_x\text{Hg}_{1-x}\text{Te}$ contact measured

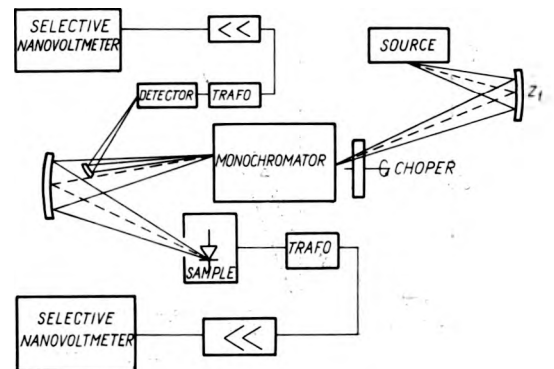


Fig. 6b. Experimental arrangement used for the measurement of contact photovoltage

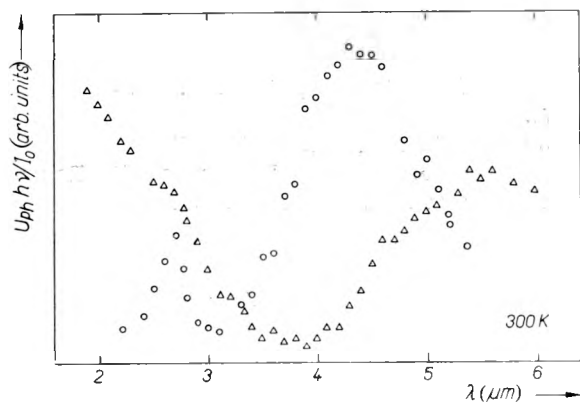


Fig. 7. Normalized photovoltage spectra of Au-(p)Cd_xHg_{1-x}Te contact in front-wall (triangles), and back-wall (circles) geometries

Vth-5/7 thermocouple. Within the wavelength region used (1–10 μm) the probable errors in energy estimation were about 10 meV.

The obtain results are shown in fig. 7 in form of normalized photovoltage spectra

$$U_{Ph} \left(\frac{h\nu}{I_0} \right) \lambda.$$

These curves being typical of our experiments show clearly the differences between PV values measured for photons illuminating the metal layers and those falling on semiconductor surface which may be explained on the basis of photon flux distribution and photoexcitation processes described above.

The photovoltage from the low-energy region (from $\lambda \cong 6 \mu\text{m}$ to $\lambda \cong 4.5 \mu\text{m}$) is concluded to be the result of the internal photoexcitation* (mechanism (c) in fig. 3). Energy threshold values are in a satisfying agreement with the energy gap value of semiconductor used (fig. 8a). In this waverange the photoresponse in a front-wall configuration is smaller than in a back-wall one due to the absorption in the metal layer and inverted region relatively higher than in semiconductor volume (see fig. 5). Long-wave threshold in a back-wall geometry is shifted to higher energy. In this case the absorption in near-surface region of semiconductor begins to play an important role. Obviously for $h\nu > E_g$, the flux falling on the surface is absorbed mainly in near-surface region.

The energy threshold values determined for photoemission of holes from Fermi level in metal into Cd_xHg_{1-x}Te over the potential barrier Φ_{BC} are presented in fig. 8b. The Φ_{BC} values obtained from photovoltage measurements are in a good agreement with

* It should be noted that the photovoltage is also possible in this case if there exist heterogeneities in the crystal.

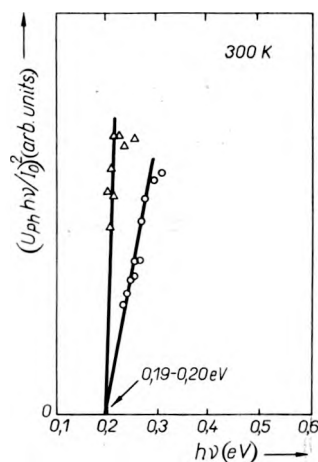


Fig. 8a. Square of normalized photovoltage as a function of photon energy for low-energy region

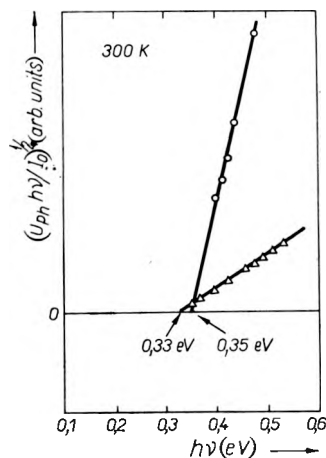


Fig. 8b. Square root of normalized photovoltage as a function of photon energy for high-energy region

the barrier height estimated from electrical transport measurements [6].

The results of PV-measurements presented above have stimulated further investigations which actually conducted.

Фотовольтаические свойства контакта металл-полупроводник с узкой запрещенной зоной

Обсужден механизм возникновения фотовольтаических спектров (распределения потоков фотонов и процессы фотовозбуждения) в контактах металл-полупроводник. Особое внимание уделено металлическим контактам к полупроводникам с узкой запрещенной зоной. Описано применение фотогальванических измерений для исследования свойств контакта металл-(p) C_xHg_{1-x}Te.

References

- [1] NILL K. W., WALPOLE J. N., CALAWA A. R., HARMAN T. C., Proc. Conf. Physics of Semimetals and Narrow-gap Semicond., Dallas 1970 (ed. D. L. Carter and R. T. Bate), Pergamon Press 1971.
- [2] PAWLIKOWSKI J. M., Phys. Stat. Sol. (a) **40**, 613, 1977.
- [3] MOSS T. S., J. Luminescence **7**, 359, 1973.
- [4] LEPPihalme M., TUOMI T., Phys. Stat. Sol. (a) **33**, 125, 1976.
- [5] FOWLER R. H., Phys. Rev. **38**, 45, 1931.
- [6] PAWLIKOWSKI J. M., BECLA P., LUBOWSKI K., ROSZKIEWICZ K., Acta Phys. Pol. A **49**, 563, 1976.

Received January 31, 1977